Production of light nuclei in isobaric Ru + Ru and Zr + Zr collisions at $\sqrt{s_{NN}} = 7.7$–200 GeV from a multiphase transport model

Fei Li (李飞) [1], Song Zhang (张松),[1,2,*] Kai-Jia Sun (孙开佳),[1,2,†] and Yu-Gang Ma (马余刚) [1,2,‡]

[1]*Key Laboratory of Nuclear Physics and Ion-beam Application (MOE), Institute of Modern Physics,*
Fudan University, Shanghai 200433, China

[2]*Shanghai Research Center for Theoretical Nuclear Physics NSFC and Fudan University, Shanghai 200438, China*

The production of light nuclei in isobaric $^{96}_{44}\text{Ru} + ^{96}_{44}\text{Ru}$ and $^{96}_{40}\text{Zr} + ^{96}_{40}\text{Zr}$ collisions, ranging from $\sqrt{s_{NN}} = 7.7$ to 200 GeV, are studied using the string melting version of a multiphase transport model in combination with a coalescence approach to light nuclei production. From the calculated yields, transverse momentum (p_T) spectra, and rapidity dependences of light nuclei (p, n, d, t, ^{3}He), we find that the Ru + Ru/Zr + Zr ratios for the yields of these particles exceed unity with the inclusion of a quadrupole deformation β_2 and octupole deformation β_3 as well as the neutron skins. We also find that heavier particles have a larger deviation from unity. Furthermore, we find that as the collision energy increases, the influence of isospin effects on the production of light nuclei in isobar collisions gradually decreases, while the influence of nuclear structure becomes more significant, particularly evident from the energy dependence of the deuteron ratio, which is unaffected by isospin effects.

I. INTRODUCTION

The study of light nuclei production in heavy-ion collisions has received increased interest both experimentally [1–6] and theoretically [7–13] due to its relevance in probing the critical point of strongly interacting matter [14–24] and indirect dark matter searches [25,26].

Light nuclei with baryon number $B \leqslant 4$, such as deuteron (d), triton (t), and helium-3 (^{3}He), are loosely bound states with binding energies significantly smaller than the temperature of the hot and dense matter created in relativistic heavy-ion collisions. Their production has been analyzed through various models, including the statistical hadronization model [27–29], the nucleon coalescence model [10,30–39], and dynamical models based on the kinetic theory [40]. In the statistical hadronization model, both light nuclei and hadrons are produced at the chemical freeze-out, characterized by a specific temperature and baryon chemical potential. In contrast, the nucleon coalescence model suggests light nuclei formation from kinetically freeze-out nucleons that are close in phase space. Dynamical models treat light nuclei as explicit degrees of freedom with their dissociation and regeneration controlled by hadronic reactions satisfying the principle of detailed balance [41–45]. Despite the great progress in recent years, the formation mechanism of light nuclei remains under debate.

Isobaric collisions like $^{96}_{44}\text{Ru} + ^{96}_{44}\text{Ru}$ and $^{96}_{40}\text{Zr} + ^{96}_{40}\text{Zr}$ [46–48] collisions aimed at the search of the anomalous phe-nomenon of chiral magnetic effect (CME) [46,49–51]. They also provide a good opportunity to investigate the impact of initial nuclear structure through its influence on final observables such as N_{ch}, v_2, v_3, etc. [52–59]. Many studies have shown that the Ru nucleus has quadrupole deformation, while the Zr nucleus has octupole deformation, and they possess different nuclear density [60,61]. This difference explains the observed differences in v_2 and v_3 ratios between the two isobaric $^{96}_{44}\text{Ru} + ^{96}_{44}\text{Ru}$ and $^{96}_{40}\text{Zr} + ^{96}_{40}\text{Zr}$ collisions at $\sqrt{s_{NN}} = 200$ GeV, as recently reported in the results from the STAR experiment [46]. In previous study on the production of light nuclei in isobar collisions, researchers employed $^{96}_{44}\text{Ru} + ^{96}_{44}\text{Ru}$ and $^{96}_{40}\text{Zr} + ^{96}_{40}\text{Zr}$ (under the assumption of identical nuclear structures) collisions to investigate the impact of the CME on the production of (anti)hypernuclei and light (anti)nuclei, and the results revealed no discernible effect [62].

In the present study, we aim to explore the effects of initial nuclear structure on the production of light nuclei in isobar collisions by taking into account the different internal structures of $^{96}_{44}\text{Ru}$ and $^{96}_{40}\text{Zr}$ nuclei. Specifically, we investigate light nuclei (d, t, ^{3}He) production at midrapidity ($|y| < 0.5$) in isobaric $^{96}_{44}\text{Ru} + ^{96}_{44}\text{Ru}$ and $^{96}_{40}\text{Zr} + ^{96}_{40}\text{Zr}$ collisions from 7.7 to 200 GeV using a coalescence approach. We explore the impact of nuclear structure and isospin on various final-state observables by employing four different sets of nuclear structure parameters for Ru and Zr. We find that the Ru + Ru/Zr + Zr ratios for yields of these particles exceed unity after accounting for a quadrupole deformation β_2 and octupole deformation β_3 as well as the neutron skin between these two isobars. We also find that the impact of isospin effects on light nuclei production in isobar collisions becomes weak as increasing the collision energy, while the influence of nuclear structure exhibits an opposite trend.

─────────

*Contact author: song_zhang@fudan.edu.cn

†Contact author: kjsun@fudan.edu.cn

‡Contact author: mayugang@fudan.edu.cn

The paper is organized as follows. In Sec. II, a multiphase transport (AMPT) model with a coalescence approach and four sets of WS parameters for Ru and Zr are briefly introduced. In Sec. III, the analysis of p_T spectra, dN/dy, particle ratios for light nuclei in isobar collisions at $\sqrt{s_{NN}} = 7.7$, 27, 62.4, and 200 GeV are presented. Finally, the summary is given in Sec. IV.

II. METHODS

A. The AMPT model and nucleon coalescence model

To study the production of deuteron (d), triton (t), and helium-3 (^{3}He) in Ru + Ru and Zr + Zr collisions at $\sqrt{s_{NN}} = 7.7$, 27, 62.4, and 200 GeV, we employ the nucleon coalescence model for cluster production with the nucleon phase-space information generated from the string melting version of AMPT model [63,64]. The AMPT model is widely used to study a variety of observables in relativistic heavy-ion collisions. It consists of four parts: the Heavy-Ion Jet INteraction Generator (HIJING) model [65,66] for generating the initial-state conditions, Zhang's parton cascade (ZPC) model [67] for modeling the partonic cascade, the Lund string fragmentation model or a quark coalescence model for hadron formation, and a relativistic transport (ART) model [68] for hadronic scatterings and decays.

In this work, we adopt a coalescence approach [19,69], in which light nuclei are formed from kinetically freeze-out nucleons that are nearby in phase space. In this approach, deuteron (d) are formed if their relative coordinate $\Delta r_{p,n}$ and momentum $\Delta p_{p,n}$ between proton (p) and neutron (n) in the two-nucleon rest frame satisfy $\Delta r_{p,n} \leqslant 3.0$ fm and $\Delta p_{p,n} \leqslant 0.16$ GeV/c simultaneously, where the $\Delta r_{p,n}$ and $\Delta p_{p,n}$ are defined as

$$\Delta r_{p,n} = |\mathbf{r}_p - \mathbf{r}_n|, \quad \Delta p_{p,n} = |\mathbf{p}_p - \mathbf{p}_n| \quad (1)$$

with the $\mathbf{r}_i$ and $\mathbf{p}_i$ being the coordinate and momentum of nucleon i, respectively. In the two-nucleon rest frame, we synchronize the freeze-out times by allowing the nucleon that freezes out earlier to freely propagate to the later freeze-out time of the other nucleon. Similarly, for the triton (t) and helium-3 (^{3}He) of the three-body system, the coalescence parameters are determined by the maximum relative distance $\Delta r_{\max}$ of the nucleon to the coordinates of the center-of-mass and the maximum relative momentum $\Delta p_{\max}$ among the nucleons. The center-of-mass coordinate $\mathbf{R}$ and the maximum relative distance $\Delta r_{\max}$ are given by

$$\mathbf{R} = \frac{\mathbf{r}_1 + \mathbf{r}_2 + \mathbf{r}_3}{3}, \quad \Delta r_{\max} = \max\{|\mathbf{R} - \mathbf{r}_i|\} \quad (i = 1, 2, 3),$$
$$(2)$$

and the maximum relative momentum $\Delta p_{\max}$ is given by

$$\Delta p_{\max} = \max\{|\mathbf{p}_i - \mathbf{p}_j|\} \quad (i \neq j; i, j = 1, 2, 3), \quad (3)$$

where the $\Delta r_{\max} \leqslant 2.0$ fm, and $\Delta p_{\max} \leqslant 0.16$ GeV/c, respectively.

Under the conditions described above, deuteron ($pn \to d$) is formed by one proton and one neutron, triton ($pnn \to t$) is composed of one proton and two neutrons, while helium-3 ($ppn \to {}^3$He) consists of two protons and one neutron. This

TABLE I. The Woods-Saxon parameters used in the AMPT model.

Nucleus	$^{96}_{44}$Ru				$^{96}_{40}$Zr			
	R_0 (fm)	a (fm)	β_2	β_3	R_0 (fm)	a (fm)	β_2	β_3
Case-1	5.096	0.540	0	0	5.096	0.540	0	0
Case-2	5.13	0.46	0.13	0	5.06	0.46	0.06	0
Case-3	5.067	0.5	0	0	4.965	0.556	0	0
Case-4	5.065	0.485	0.154	0	4.961	0.544	0.062	0.202

simple coalescence model is found to describe successfully the experimental data in collisions considered in the present study.

B. Geometric description of $^{96}_{44}$Ru and $^{96}_{40}$Zr

In AMPT, the spatial distribution of nucleons within $^{96}_{44}$Ru and $^{96}_{40}$Zr is characterized by the Woods-Saxon (WS) distribution [47,70,71] function as follows:

$$\rho(r, \theta) = \frac{\rho_0}{1 + \exp\left[\frac{r - R_0\left(1 + \beta_2 Y_2^0(\theta) + \beta_3 Y_3^0(\theta)\right)}{a}\right]}, \quad (4)$$

where r is radial distance from the center and θ is polar angle in spherical coordinates. The parameters R_0 and a represent the "radius" of the nucleus and the surface diffuseness parameter, respectively. The value of ρ_0 in Eq. (4) is determined from the nucleon number A. The nuclear shape deformations are characterized by the axial symmetric quadrupole deformation parameter β_2 and the octupole deformation parameter β_3, which are the most significant for describing the nucleus's deformation.

In the present study, we utilize four sets of Woods-Saxon parameters to characterize the initial nucleon distribution in isobars. These parameters are widely recognized and have been adopted from a variety of recent studies [47,60,61,72–77]. The specific values for these parameters are listed in Table I. This approach allows us to systematically investigate the impact of nuclear structure variations on the production of light nuclei in isobaric collisions.

The parameters for the initial nucleon distributions are organized into four cases: Case-1 assumes identical values for a and R_0 for both Ru and Zr, with no deformation present in either nucleus; Case-2 differentiates the two nuclei by their quadrupole deformation with Ru ($\beta_2^{Ru} = 0.13$) exhibiting a larger deformation than Zr ($\beta_2^{Zr} = 0.06$); Case-3, as referenced from [61,78], posits both nuclei as spherical ($\beta_2 = 0$). Here, variations in R_0 and a suggest that Ru is overall smaller than Zr, largely due to Zr having a more substantial neutron skin; Case-4 provides a comprehensive description of the nuclear structure, encompassing both the deformation effect (β_2 and β_3) [60,75] and the neutron skin effect for $^{96}_{44}$Ru and $^{96}_{40}$Zr, which leads to the best description of $v_{2,Ru}/v_{2,Zr}$ in isobar collisions at $\sqrt{s_{NN}} = 200$ GeV [79]. It should be noted that we use the total nucleon density (the sum of the proton and neutron) to represent the neutron skin effect caused by different density distributions of proton and neutron. The feasibility of this approach is supported by previous research [61], which has shown that the Ru + Ru/Zr + Zr ratio remains consis-
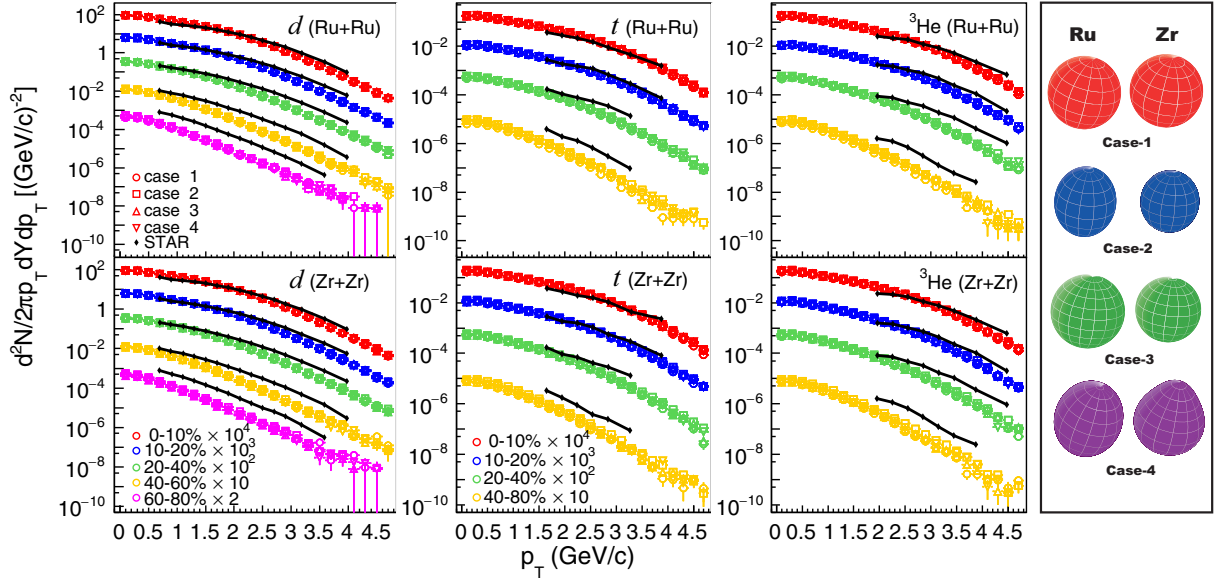
FIG. 1. Transverse momentum spectra for d ($|y| < 0.35$), t ($|y| < 0.5$), and ^{3}He ($|y| < 0.5$) in 0–10 %, 10–20 %, 20–40 %, 40–60 %, and 60–80 % (40–80 % for t and ^{3}He) isobaric collisions at $\sqrt{s_{NN}} = 200$ GeV with four different sets of Woods-Saxon parameters. The STAR data (black solid lines) for isobar collisions at $\sqrt{s_{NN}} = 200$ GeV [80] are also shown for comparisons.

tent when comparing calculations using distinct proton and neutron densities in energy density functional theory (DFT) calculations with those using total nucleon density in WS parameters.

III. RESULTS AND DISCUSSION

The results from the AMPT model with a coalescence approach for four sets of WS parameters in Ru + Ru and Zr + Zr collisions at $\sqrt{s_{NN}} = 7.7$, 27, 62.4, and 200 GeV are presented, as well as for the STAR data on isobar collisions at $\sqrt{s_{NN}} = 200$ GeV for comparisons. We will show the predictions for the transverse momentum p_T spectra, the particle yield dN/dy, and the particle ratios of light nuclei as a function of centrality at mid-rapidity in isobar collisions. We will also discuss the energy dependence of the effects of isospin and nuclear structure on the ratios of these observations between the two collision systems. The numbers of events we simulated for all cases for both $^{96}_{44}$Ru and $^{96}_{40}$Zr are, respectively, 5M (7.7 GeV), 4M (27 GeV), 3.5M (62.4 GeV), and 5M (200 GeV), where M denotes $\times 10^6$.

A. The p_T spectra of light nuclei

Shown in Fig. 1 are the transverse momentum p_T spectra of deuterons (d, $|y| < 0.35$), tritons (t, $|y| < 0.5$), and helium-3 (^{3}He, $|y| < 0.5$) in Ru + Ru and Zr + Zr collisions. The spectra are shown across various centrality bins: 0–10 %, 10–20 %, 20–40 %, 40–60 %, and 60–80 % (40–80 % for t and ^{3}He) using four different WS parameter sets. For comparison, the STAR data on these light nuclei in isobar collisions at $\sqrt{s_{NN}} = 200$ GeV is also included.

The p_T spectra of deuterons (d), tritons (t), and helium-3 (^{3}He) with four different sets of WS parameters agree well with STAR data in the central collision region (0–10 % and 10–20 %). However, in the more peripheral collisions (40–60 % and 60–80 %), the obtained yields underestimate the STAR data. The underestimation of light nuclei production in peripheral collisions results from the imperfection of the hadron production mechanism in the AMPT model in peripheral collisions or small system collisions, which needs further improvement but is beyond the scope of this work. Fortunately, this issue does not affect the following defined ratios significantly.

B. The yields of light nuclei

Figure 2 depicts the yields (dN/dy) of p, n, d, t, and ^{3}He at midrapidity ($|y| < 0.5$) as a function of centrality in Ru + Ru and Zr + Zr collisions at $\sqrt{s_{NN}} = 7.7$ and 200 GeV, utilizing four sets of WS parameters. For subsequent analysis, the rapidity of deuterons is constrained to $|y| < 0.5$. Additionally, the STAR data on the rapidity density (dN/dy) for d, t, and ^{3}He in isobar collisions [80], as well as protons from Au + Au collisions [81], selected from a similar multiplicity collision region (10–80 %) as isobar collisions, at $\sqrt{s_{NN}} = 200$ GeV, are presented for comparison. With the four sets of WS parameters, both the dN/dy of each particle are consistent between Ru + Ru and Zr + Zr collisions at $\sqrt{s_{NN}} = 7.7$ and 200 GeV. The dN/dy of four cases all exhibit a decreasing trend from central to peripheral collisions at both collision energies.

The yields (dN/dy) of light nuclei are shown in the upper panels and the Ru + Ru/Zr + Zr ratio of dN/dy for p, n, d, t, and ^{3}He at $\sqrt{s_{NN}} = 200$ and 7.7 GeV in the middle panels and the lower panels, respectively. For the Ru + Ru/Zr + Zr
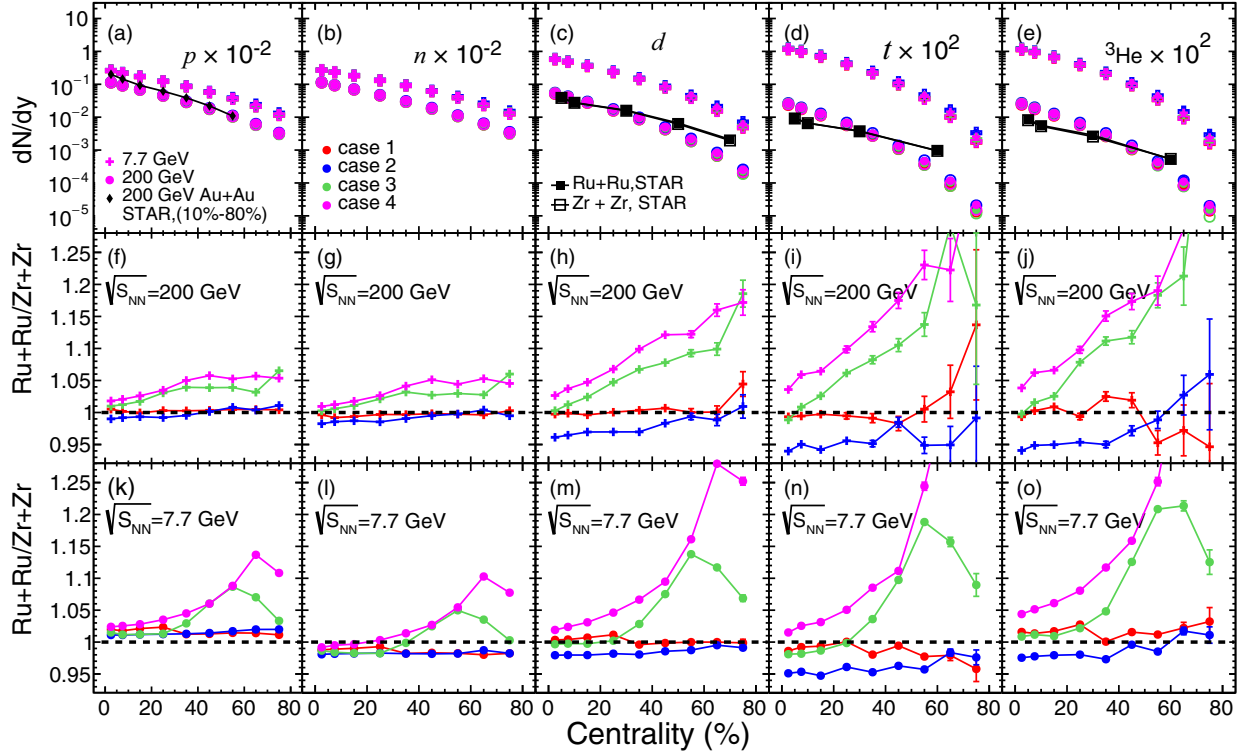
FIG. 2. The rapidity density (dN/dy) of p, n, d, t, and ^{3}He at midrapidity ($|y| < 0.5$) versus the centrality in Ru + Ru and Zr + Zr collisions at $\sqrt{s_{NN}} = 7.7$ and 200 GeV for four cases of WS parameters. dN/dy of p, n, and t, ^{3}He are scaled with factors of 0.01 and 100 for better representation, respectively. The STAR data for d, t, and ^{3}He in isobar collisions [80], as well as p from Au + Au collisions (10–80 %) [81] at $\sqrt{s_{NN}} = 200$ GeV, are also shown for comparisons. Ru is represented by solid symbols and Zr by open symbols. The Ru + Ru/Zr + Zr ratio of dN/dy is shown in the lower panels for $\sqrt{s_{NN}} = 7.7$ and 200 GeV, respectively.

ratios of p and n [as illustrated in Figs. 2(f) and 2(g)], their values remain near unity across all centralities at 200 GeV in Case 1, where the $^{96}_{44}$Ru and $^{96}_{40}$Zr nuclei are the same nuclear size and without deformation. In Case 2, which incorporates larger quadrupole deformation of $^{96}_{44}$Ru compared to $^{96}_{40}$Zr, the Ru + Ru/Zr + Zr ratios of p and n slightly dip below unity within central collision regions at 200 GeV. Conversely, in Cases 3 and 4, the Ru + Ru/Zr + Zr ratios of p and n ratios almost linearly increase with centrality. Specifically, the ratios in Case 4, which considers both quadrupole and octupole deformation as well as the neutron skin effect, exceed those in Case 3 which accounts only for the neutron skin effect. For d, t, and ^{3}He, depicted in Figs. 2(h), 2(i), and 2(j), their Ru + Ru/Zr + Zr ratios exhibit a similar trend to those of p and n but with more pronounced deviations from unity in Cases 2, 3, and 4.

The reason for a larger particle yield in $^{96}_{44}$Ru + $^{96}_{44}$Ru collisions compared to $^{96}_{40}$Zr + $^{96}_{40}$Zr collisions in Cases 3 and 4, both of which involve the neutron skin effect, is that $^{96}_{44}$Ru nuclei has a tighter nuclear geometry than $^{96}_{40}$Zr nuclei in the nonperipheral collision region, as the size of $^{96}_{44}$Ru is overall smaller than that of $^{96}_{40}$Zr. This leads to more participating nucleons in $^{96}_{44}$Ru + $^{96}_{44}$Ru collisions than $^{96}_{40}$Zr + $^{96}_{40}$Zr collisions, and as we know the yield of the final particle is related

to participating nucleon number N_{part} [60,61]. Comparing Case 2 (which includes deformation effects) with Case 1 (which has no nuclear structure effect), and Case 4 (which includes both deformation and neutron skin effects) with Case 3 (which includes only the neutron skin effect), it is clear that the trend in the ratios reflects the yield differences in the isobar system caused by pure deformation effects. In this system, nuclei with more deformation have lower yields, indicating that the greater the deformation of the nucleus, the smaller the initial nucleon number. This is consistent with the results in [46,60,61].

At a lower energy of $\sqrt{s_{NN}} = 7.7$ GeV, the proton (p) ratio mostly increases for all cases relative to the results at 200 GeV, while the neutron (n) ratio mostly decreases relative to the result at 200 GeV, as shown in Figs. 2(k) and 2(l). This is different from the trend observed at 200 GeV, where the p and n ratios were almost identical. Compared to the initial $^{96}_{44}$Ru + $^{96}_{44}$Ru collision system, the initial $^{96}_{40}$Zr + $^{96}_{40}$Zr collision system had a higher neutron-to-proton ratio (n/p). The difference of Ru + Ru/Zr + Zr ratio between the p and n at different energies indicates the isospin effect on the yield ratio of p and n at lower collision energy have a more significant impact, and this influence is attenuated at higher energy.
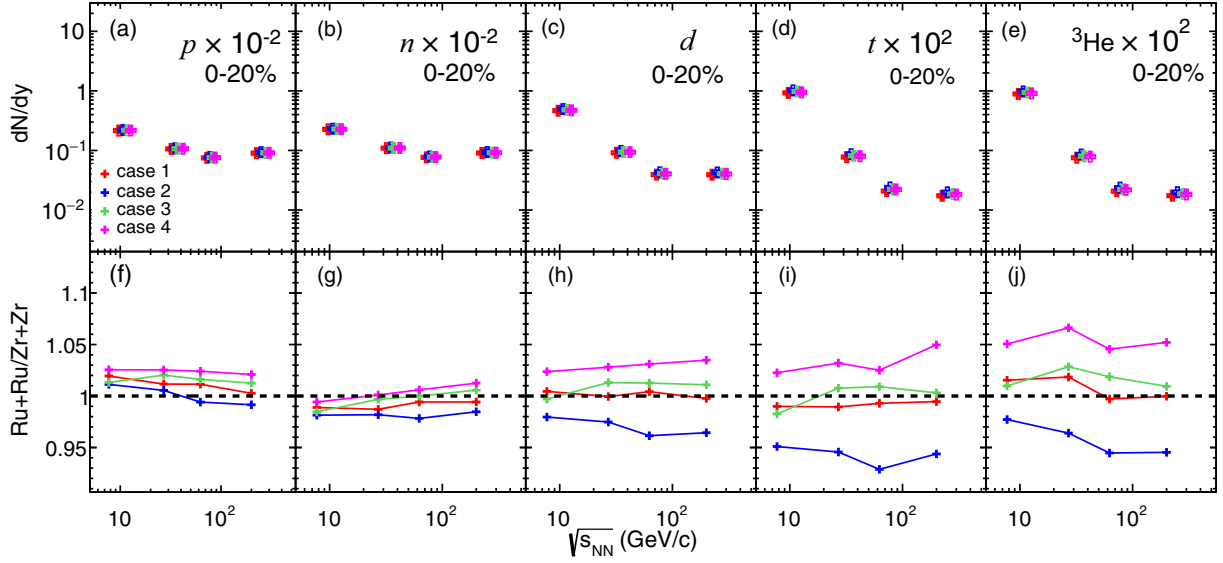
FIG. 3. The rapidity density (dN/dy) of p, n, d, t, and ^{3}He at midrapidity ($|y| < 0.5$) in the central isobar collisions as a function of energy for four cases of WS parameters. dN/dy of p, n, t, and ^{3}He are scaled with factors of 0.01 and 100 for better representation, respectively. Ru is represented by solid symbols and Zr by open symbols. The Ru + Ru/Zr + Zr ratio of dN/dy is shown in the lower panels.

C. The yields energy dependence of light nuclei

Figure 3 presents the yields energy dependence of p, n, d, t, and ^{3}He in central collisions (0–20 %). With increasing energy, a trend is observed where the ratio for protons (p) in Case 1 decreases towards unity, while the ratio for neutrons (n) increases towards unity. This suggests an amplification of the isospin effect in isobar collisions at lower energies.

Additionally, as shown in Fig. 3(h), the ratio for deuterons (d, consisting of $p-n$ pairs) in Case 1 remains constant at unity across different energies, suggesting that the production mechanism of $p-n$ paired for deuteron is unaffected by the isospin differences between $^{96}_{44}$Ru + $^{96}_{44}$Ru and $^{96}_{40}$Zr + $^{96}_{40}$Zr collisions. Conversely, as depicted in Fig. 3(i), the triton (t, consisting of pnn) ratio in Case 1 exhibits a trend similar to that of neutrons, while Fig. 3(j) demonstrates that the ratio for helium-3 (^{3}He, consisting of ppn) in Case 1 follows the trend of protons, implying their Ru + Ru/Zr + Zr ratio are influenced by the excess nucleon relative to the $p-n$ pair.

Considering that the Ru + Ru/Zr + Zr ratio of deuteron is not affected by isospin effects in Case 1, where $^{96}_{44}$Ru and $^{96}_{40}$Zr nuclei have the same nuclear structure, the additional cases depicted in Fig. 3(h) offer the potential to understand the energy dependence of the nuclear structure on light nuclei production. In Cases 2 and 4, the effect of nuclear structure on yield ratio increases with energy. Case 3 displays nonmonotonicity; this is because the neutron skin effect's influence on yield ratios is predominantly observed in midcentral collisions [60,79,82]. Therefore, the results for Case 3 in the central collision region may not accurately reflect the energy dependence of the neutron skin effect.

Furthermore, in Fig. 3(f), the energy dependence of the ratios for protons (p) in Case 4 remains almost constant. This is attributed to the interplay between nuclear structure and isospin effects at varying energies, with their energy dependencies exhibiting contrasting behaviors.

D. The ratios of light nuclei

Figure 4 depicts the particle ratios d/p, t/p, ^{3}He$/p$, t/d, and $t/^3$He at midrapidity ($|y| < 0.5$) verse the centrality for $^{96}_{44}$Ru + $^{96}_{44}$Ru and $^{96}_{40}$Zr + $^{96}_{40}$Zr collisions at $\sqrt{s_{NN}} = 7.7$ GeV and 200 GeV, using four sets of WS parameters. The particle ratios d/p, t/p, ^{3}He$/p$, and t/d consistently decrease from central to peripheral collisions for all cases at $\sqrt{s_{NN}} = 7.7$ GeV and 200 GeV.

Notably, for all cases, the particle ratio d/p (pn/p) closely aligns with t/d (pnn/pn), and similarly, t/p (pnn/p) is close to ^{3}He$/p$ (ppn/p). This can be attributed to the fact that they correspond to the same nucleon component multiples. Specifically, the ratios of both d/p and t/d correspond to the nucleon component p, while t/p and ^{3}He$/p$ are associated with nn and pn, respectively.

The lower panels of Fig. 4 depict the ratio between Ru + Ru and Zr + Zr collisions of the above particle ratios at $\sqrt{s_{NN}} = 200$ GeV and 7.7 GeV for all cases. In Case 1, where there are no nuclear structure differences between $^{96}_{44}$Ru and $^{96}_{40}$Zr, all Ru + Ru/Zr + Zr ratios of particle ratios converge to unity in central collisions at $\sqrt{s_{NN}} = 200$ GeV. In contrast, variations in these ratios are evident (except for d/p and t/d being the same) across all centralities at $\sqrt{s_{NN}} = 7.7$ GeV. The difference between $\sqrt{s_{NN}} = 200$ and 7.7 GeV can be attributed to a stronger isospin effect at the lower energy, as we stated before. The Ru + Ru/Zr + Zr ratios of d/p and t/d remain the same at the lower energy because they have the same nucleon component p, while t/p and ^{3}He$/p$ separate at lower energy for they possess different nucleon components. The above results are also consistent with other cases involving nuclear structure, where the ratios of d/p and t/d
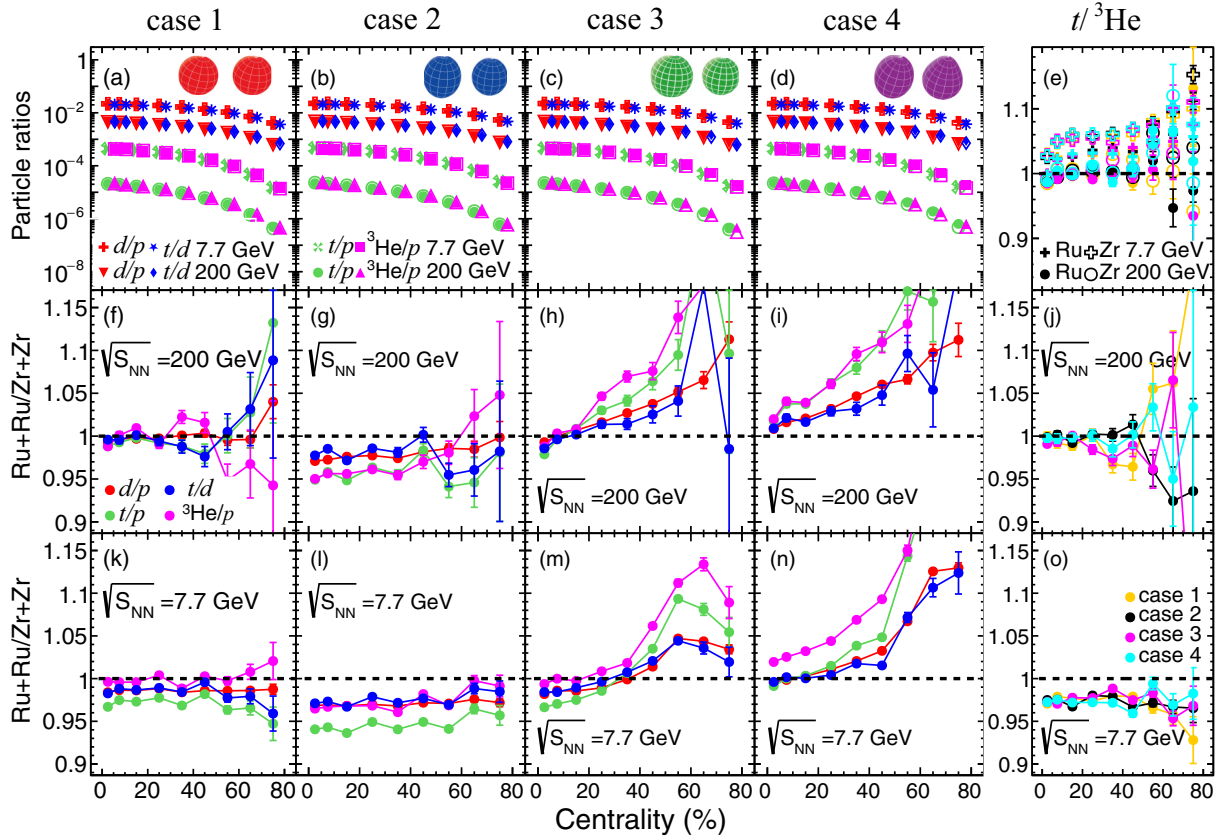
FIG. 4. The particle ratios of d/p, t/p, ^{3}He/p, t/d, and $t/^3$He at midrapidity ($|y| < 0.5$) versus the centrality in Ru + Ru and Zr + Zr collisions at $\sqrt{s_{NN}} = 7.7$ and 200 GeV for four cases of WS parameters. Ru is represented by solid symbols and Zr by open symbols. The Ru + Ru/Zr + Zr ratio of particle ratios is shown in the lower panels for $\sqrt{s_{NN}} = 7.7$ and 200 GeV, respectively.

consistently remain the same. Conversely, the ratios of t/p and ^{3}He/p exhibit a proximity at $\sqrt{s_{NN}} = 200$ GeV, while displaying a difference at lower energy of 7.7 GeV. This can be seen more clearly in the results of the energy dependence of yields ratio in Fig. 5.

In addition, Fig. 4(e) shows that the yield ratio $t/^3$He is close to unity in central collisions and increases to 1.1 in peripheral collisions. However, we note that this ratio is much larger (about 1.8) in the preliminary result from STAR [80], although the uncertainty is significantly large. In Figs. 4(j), and 4(o), the Ru + Ru/Zr + Zr ratios of $t/^3$He for four cases of WS parameters at $\sqrt{s_{NN}} = 200$ GeV and 7.7 GeV are close to each other because of the cancellation of nuclear structure with the same nucleon component for triton and ^{3}He. It is also shown in Fig. 5(j) that the equivalent Ru + Ru/Zr + Zr ratio of $t/^3$He converges to unity as the energy increases for all cases. This further corroborates that the impact of the initial isospin differences on the isobar collision system weakens with increasing energy.

IV. CONCLUSION AND OUTLOOK

We investigate p_T spectra, dN/dy, and particle ratios for p, n, d, t, and ^{3}He at midrapidity ($|y| < 0.5$) in $^{96}_{44}$Ru+$^{96}_{44}$Ru and $^{96}_{40}$Zr+$^{96}_{40}$Zr collisions at $\sqrt{s_{NN}} = 7.7$, 27, 62.4, and 200 GeV using the AMPT model combined with a final-state

coalescence model for light nuclei production. Using four sets of WS parameters for $^{96}_{44}$Ru and $^{96}_{44}$Zr, the effect of nuclear structure and isospin on the production of light nuclei in isobaric collisions and the energy dependence of this effect are investigated.

We find that there is little difference in dN/dy and particle ratios for each particle between collisions of $^{96}_{44}$Ru + $^{96}_{44}$Ru and $^{96}_{40}$Zr + $^{96}_{40}$Zr at 200 GeV when assuming identical nuclear structures for $^{96}_{44}$Ru and $^{96}_{40}$Zr. A difference in dN/dy and particle ratios is observed between isobar collisions when these two nuclei possess distinct nuclear structures. A maximum deviation from unity in the Ru + Ru/Zr + Zr ratio of dN/dy and particle ratios is observed for each particle at 200 GeV when considering the nuclear structure with quadrupole deformation β_2, octupole deformation β_3, and neutron skin for $^{96}_{44}$Ru and $^{96}_{40}$Zr nuclei. We also found that the heavier particles exhibit greater deviations from unity in the dN/dy and particle ratios between isobar collisions, which is consistent with the results of Ref. [59].

In addition, we find that the impact of initial isospin on light nuclei production in isobar collisions weakens with increasing collision energy, while the effect of nuclear structure exhibits an opposite trend. This can be seen in the behavior of deuteron in Cases 1, 2, and 4 as shown in Fig. 3. Furthermore, we find that the value of $t/^3$He in peripheral collisions is about 1.1 which is, however, much lower than the preliminary
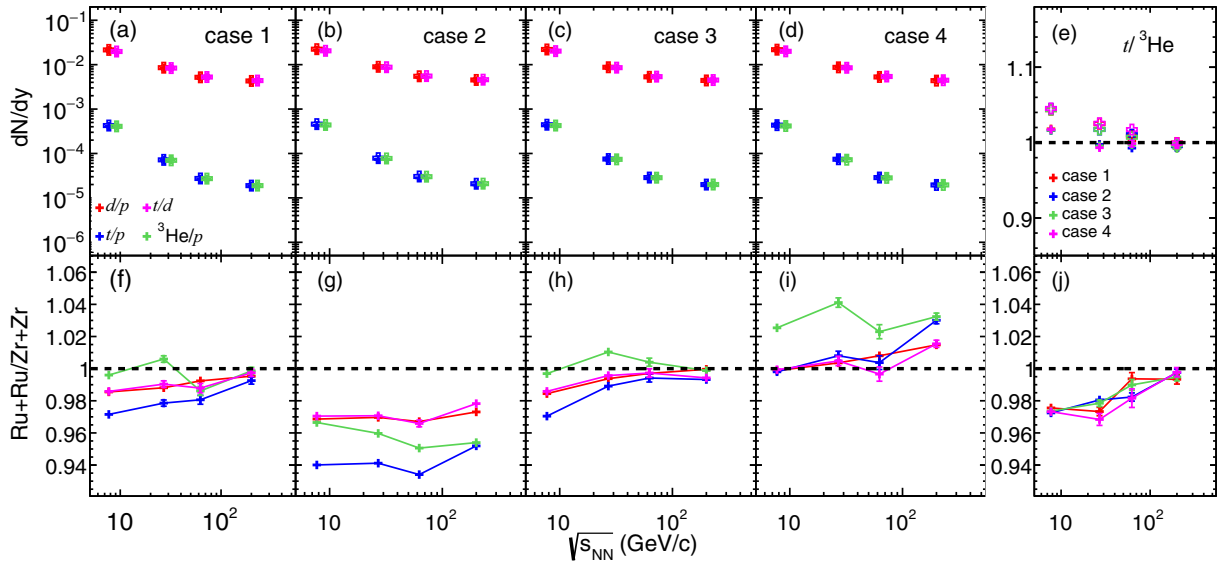
FIG. 5. The particle ratios of d/p, t/p, ^{3}He$/p$, t/d, and $t/^3$He at midrapidity ($|y| < 0.5$) in the central isobar collisions as a function of energy for four cases of WS parameters. Ru is represented by solid symbols and Zr by open symbols. The Ru + Ru/Zr + Zr ratio of particle ratios is shown in the lower panels.

result of about 1.8 reported by STAR [80] although with significant uncertainty. Our results can be tested in upcoming data from the STAR Collaboration and may provide a deeper understanding of the formation mechanism of light nuclei as well as the effects of internal structures of colliding nuclei.

[1] V. T. Cocconi, T. Fazzini, G. Fidecaro, M. Legros, N. H. Lipman, and A. W. Merrison, Phys. Rev. Lett. **5**, 19 (1960).

[2] J. Adam, L. Adamczyk, J. Adams, J. Adkins, G. Agakishiev, M. Aggarwal, Z. Ahammed, I. Alekseev, D. Anderson, R. Aoyama *et al.* (STAR Collaboration), Phys. Rev. C **99**, 064905 (2019).

[3] D. Zhang, S. Collaboration *et al.*, Nucl. Phys. A **1005**, 121825 (2021).

[4] J. Chen, D. Keane, Y.-G. Ma, A. Tang, and Z. Xu, Phys. Rep. **760**, 1 (2018).

[5] A. Ono, Prog. Part. Nucl. Phys. **105**, 139 (2019).

[6] Y. Zhang, D. W. Zhang, and X. F. Luo, Nucl. Tech. **46**, 040001 (2023).

[7] D. Oliinychenko, Nucl. Phys. A **1005**, 121754 (2021).

[8] P. Braun-Munzinger and B. Dönigus, Nucl. Phys. A **987**, 144 (2019).

[9] L. Csernai and J. I. Kapusta, Phys. Rep. **131**, 223 (1986).

[10] K.-J. Sun, L.-W. Chen, C. M. Ko, J. Pu, and Z. Xu, Phys. Lett. B **781**, 499 (2018).

[11] C. B. Dover, U. Heinz, E. Schnedermann, and J. Zimányi, Phys. Rev. C **44**, 1636 (1991).

[12] K. J. Sun, L. W. Chen, C. M. Ko, F. Li, J. Xu, and Z. B. Xu, Nucl. Tech. **46**, 040012 (2023).

[13] Q. Chen, G. L. Ma, and J. H. Chen, Nucl. Tech. **46**, 040013 (2023).

[14] M. Abdulhamid *et al.* (STAR Collaboration), Phys. Rev. Lett. **130**, 202301 (2023).

[15] K.-J. Sun, L.-W. Chen, C. M. Ko, and Z. Xu, Phys. Lett. B **774**, 103 (2017).

[16] E. Shuryak and J. M. Torres-Rincon, Phys. Rev. C **101**, 034914 (2020).

[17] N. Yu, D. Zhang, and X. Luo, Chin. Phys. C **44**, 014002 (2020).

[18] T. Shao, J. Chen, C. M. Ko, and K.-J. Sun, Phys. Lett. B **801**, 135177 (2020).

[19] X.-G. Deng and Y.-G. Ma, Phys. Lett. B **808**, 135668 (2020).

[20] W. Zhao, C. Shen, C. M. Ko, Q. Liu, and H. Song, Phys. Rev. C **102**, 044912 (2020).

[21] H. Liu, D. Zhang, S. He, K.-J. Sun, N. Yu, and X. Luo, Phys. Lett. B **805**, 135452 (2020).

[22] C. M. Ko, Nucl. Sci. Tech. **34**, 80 (2023).

[23] W.-B. He, Y.-G. Ma, L.-G. Pang, H.-C. Song, and K. Zhou, Nucl. Sci. Tech. **34**, 88 (2023).

[24] Y.-G. Ma, L.-G. Pang, R. Wang, and K. Zhou, Chin. Phys. Lett. **40**, 122101 (2023).

[25] V. Vagelli, Nuovo Cimento C **42**, 173 (2019).

[26] K. Blum, Kenny Chun Yu Ng, R. Sato, and M. Takimoto, Phys. Rev. D **96**, 103021 (2017).

[27] J. Cleymans and H. Satz, Z. Phys. C **57**, 135 (1993).

[28] A. Andronic, P. Braun-Munzinger, J. Stachel, and H. Stöcker, Phys. Lett. B **697**, 203 (2011).

[29] P. Braun-Munzinger, V. Koch, T. Schäfer, and J. Stachel, Phys. Rep. **621**, 76 (2016).

[30] S. T. Butler and C. A. Pearson, Phys. Rev. **129**, 836 (1963).

[31] H. Sato and K. Yazaki, Phys. Lett. B **98**, 153 (1981).

[32] K.-J. Sun and L.-W. Chen, Phys. Rev. C **95**, 044905 (2017).

[33] N. Shah, Y. Ma, J. Chen, and S. Zhang, Phys. Lett. B **754**, 6 (2016).

[34] T. Z. Yan, Y. G. Ma, X. Z. Cai *et al.*, Phys. Lett. B **638**, 50 (2006).

[35] T.-T. Wang, Y.-G. Ma, and S. Zhang, Phys. Rev. C **107**, 014911 (2023).

[36] Y.-X. Zhang, S. Zhang, and Y.-G. Ma, Eur. Phys. J. A **59**, 72 (2023).

[37] C. Liu, X.-G. Deng, and Y.-G. Ma, Nucl. Sci. Tech. **33**, 52 (2022).

[38] Y.-L. Cheng, S. Zhang, and Y.-G. Ma, Eur. Phys. J. A **57**, 330 (2021).

[39] F. H. Qiao, X. G. Deng, and Y. G. Ma, Phys. Lett. B **850**, 138535 (2024).

[40] P. Danielewicz and G. F. Bertsch, Nucl. Phys. A **533**, 712 (1991).

[41] Y. Oh, Z.-W. Lin, and C. M. Ko, Phys. Rev. C **80**, 064902 (2009).

[42] S. Cho, T. Song, and S. H. Lee, Phys. Rev. C **97**, 024911 (2018).

[43] D. Oliinychenko, L.-G. Pang, H. Elfner, and V. Koch, Phys. Rev. C **99**, 044907 (2019).

[44] R. Wang, Y.-G. Ma, L.-W. Chen, C. M. Ko, K.-J. Sun, and Z. Zhang, Phys. Rev. C **108**, L031601 (2023).

[45] K.-J. Sun, R. Wang, C. M. Ko, Y.-G. Ma, and C. Shen, Nat. Commun. **15**, 1074 (2024).

[46] M. S. Abdallah *et al.* (STAR Collaboration), Phys. Rev. C **105**, 014901 (2022).

[47] W.-T. Deng, X.-G. Huang, G.-L. Ma, and G. Wang, Phys. Rev. C **94**, 041901(R) (2016).

[48] P. Tribedy (STAR Collaboration), J. Phys.: Conf. Ser. **1602**, 012002 (2020).

[49] D. E. Kharzeev and J. Liao, Nat. Rev. Phys. **3**, 55 (2021).

[50] M. I. Abdulhamid *et al.* (STAR Collaboration), Phys. Rev. X **14**, 011028 (2024).

[51] C.-Z. Wang, W.-Y. Wu, Q.-Y. Shou, G.-L. Ma, Y.-G. Ma, and S. Zhang, Phys. Lett. B **820**, 136580 (2021).

[52] Hao-jie Xu, EPJ Web Conf. **276**, 06020 (2023).

[53] Y.-L. Cheng, S. Shi, Y.-G. Ma, H. Stöcker, and K. Zhou, Phys. Rev. C **107**, 064909 (2023).

[54] B.-S. Xi, X.-G. Deng, S. Zhang, and Y.-G. Ma, Eur. Phys. J. A **59**, 33 (2023).

[55] S. Zhao, H.-J. Xu, Y.-X. Liu, and H. Song, Phys. Lett. B **839**, 137838 (2023).

[56] H.-J. Xu, W. Zhao, H. Li, Y. Zhou, L.-W. Chen, and F. Wang, Phys. Rev. C **108**, L011902 (2023).

[57] J. Jia, G. Giacalone, and C. Zhang, Phys. Rev. Lett. **131**, 022301 (2023).

[58] M. Nie, C. Zhang, Z. Chen, L. Yi, and J. Jia, Phys. Lett. B **845**, 138177 (2023).

[59] P. Sinha, V. Bairathi, K. Gopal, C. Jena, and S. Kabana, Phys. Rev. C **108**, 024911 (2023).

[60] J. Jia and C. Zhang, Phys. Rev. C **107**, L021901 (2023).

[61] H.-J. Xu, H. Li, X. Wang, C. Shen, and F. Wang, Phys. Lett. B **819**, 136453 (2021).

[62] Z.-L. She, G. Chen, D.-M. Zhou, L. Zheng, Y.-L. Xie, and H.-G. Xu, Phys. Rev. C **103**, 014906 (2021).

[63] Z.-W. Lin, C. M. Ko, B.-A. Li, B. Zhang, and S. Pal, Phys. Rev. C **72**, 064901 (2005).

[64] Z.-W. Lin and L. Zheng, Nucl. Sci. Tech. **32**, 113 (2021).

[65] X.-N. Wang and M. Gyulassy, Phys. Rev. D **44**, 3501 (1991).

[66] M. Gyulassy and X.-N. Wang, Comput. Phys. Commun. **83**, 307 (1994).

[67] B. Zhang, Comput. Phys. Commun. **109**, 193 (1998).

[68] B.-A. Li and C. M. Ko, Phys. Rev. C **52**, 2037 (1995).

[69] S. Sombun, K. Tomuang, A. Limphirat, P. Hillmann, C. Herold, J. Steinheimer, Y. Yan, and M. Bleicher, Phys. Rev. C **99**, 014901 (2019).

[70] G. Giacalone, J. Jia, and C. Zhang, Phys. Rev. Lett. **127**, 242301 (2021).

[71] Q. Y. Shou, Y. G. Ma, P. Sorensen, A. H. Tang, F. Videbak, and H. Wang, Phys. Lett. B **749**, 215 (2015).

[72] S. Raman, C. W. Nestor, and P. Tikkanen, At. Data Nucl. Data Tables **78**, 1 (2001).

[73] B. Pritychenko, M. Birch, B. Singh, and M. Horoi, At. Data Nucl. Data Tables **107**, 1 (2016).

[74] P. Moller, J. Nix, W. Myers, and W. Swiatecki, At. Data Nucl. Data Tables **59**, 185 (1995).

[75] G. Nijs and W. van der Schee, SciPost Phys. **15**, 041 (2023).

[76] H. Li, H.-J. Xu, J. Zhao, Z.-W. Lin, H. Zhang, X. Wang, C. Shen, and F. Wang, Phys. Rev. C **98**, 054907 (2018).

[77] J. Hammelmann, A. Soto-Ontoso, M. Alvioli, H. Elfner, and M. Strikman, Phys. Rev. C **101**, 061901(R) (2020).

[78] H.-J. Xu, X. Wang, H. Li, J. Zhao, Z.-W. Lin, C. Shen, and F. Wang, Phys. Rev. Lett. **121**, 022301 (2018).

[79] F. Li, Y.-G. Ma, S. Zhang, G.-L. Ma, and Q. Shou, Phys. Rev. C **106**, 014906 (2022).

[80] H. Liu (STAR Collaboration), Acta Phys. Pol. Suppl. **16**, 1 (2023).

[81] B. I. Abelev, M. M. Aggarwal, Z. Ahammed, B. D. Anderson (STAR Collaboration) *et al.*, Phys. Rev. C **79**, 034909 (2009).

[82] C. Zhang and J. Jia, Phys. Rev. Lett. **128**, 022301 (2022).